Influence of Shock Wave Propagation on Dielectric Barrier Discharge Plasma Actuator Performance

R. Erfani, H. Zare-Behtash, and K. Kontis*

School of Mechanical, Aerospace and Civil Engineering, University of Manchester, UK

Abstract

Interest in plasma actuators as active flow control devices is growing rapidly due to their lack of mechanical parts, light weight, and high response frequency. Although the flow induced by these actuators has received much attention, the effect that the external flow has on the performance of the actuator itself must also be considered, specially the influence of unsteady high-speed flows which are fast becoming a norm in the operating flight envelopes. The primary objective of the current study is to examine the characteristics of a dielectric barrier discharge (DBD) plasma actuator when exposed to an unsteady flow generated by a shock tube. This type of flow, which is often used in different studies, contains a range of flow regimes from sudden pressure and density changes to relatively uniform high-speed flow regions. A small circular shock tube is employed along with the schlieren photography technique to visualise the flow. The voltage and current traces of the plasma actuator are monitored throughout, and using the well established shock tube theory the change in the actuator characteristics are related to the physical processes which occur inside the shock tube. The results show that not only is the shear layer outside of the shock tube affected by the plasma but the passage of the shock front and high-speed flow behind it also greatly influences the properties of the plasma.

Keywords: Plasma actuator, Dielectric Barrier Discharge, Plasma morphology, Shock wave

*k.kontis@manchester.ac.uk.

I. INTRODUCTION

Plasma actuators have attracted much attention in the field of flow control for different speed regimes and they have been extensively studied over the last decade.[1,2] The main advantages of these flow control devices in addition to their low-power consumption are their simplicity, having near instantaneous response and having no moving parts in their structure.

The low power plasmas, such as glow discharges, coronas and dielectric barrier discharges (DBDs) have been extensively used in several low Mach number flow investigations. Particularly, DBD plasma actuators show their ability in boundary layer control,[3–7] delaying the separation on airfoils and turbine blades,[8,9] and manipulation of the laminar to turbulent transition point.[10] They consist of electrode pairs separated by a thin dielectric insulator. Supplying a high-voltage ac, typically in the range of 2-40 kV_{p-p} (peak to peak), and low current ($\sim$mA) to the electrodes weakly ionizes the air in their vicinity.

The detailed application of plasmas in the aerodynamics of flight in both low- and high-speed flow regimes suggest that weak ionization can modify aerodynamic properties of the gas flows.[11–14] Specifically, in high-speed flows, several experimental studies have demonstrated the influence of the plasma on shock wave.[15–18] Many of these investigations have been performed with shock waves, generated by an electrically pulsed discharge, propagating along the low-pressure-unconstricted dc glow discharge. It has been observed that the creation of a double layer and associated gas heating caused by the propagating shock wave can increase the shock velocity and broaden its width. Bletzinger et al.[19] found that DBDs are more efficient in producing these effects in comparison to dc glow discharge actuators. In addition, they can operate over a wide range of environmental pressures making them more desirable for flow control applications.

Although most of the studies performed focus on the influence of the plasma actuators on the flow, there have been limited investigations on the effect of the shock wave and accompanying unsteady flow on the actuator performance.[20] This is particularly important for improving the performance of the actuators in high-speed flow control applications. This will help understand the actuator capabilities and limitations when mutual interaction between the flow and actuator is considered. The present investigation is dedicated to measurements of the characteristics of a DBD plasma actuator subject to not only the

shock wave but also the unsteady high-speed flow inside the shock tube.

II. APPARATUS AND INSTRUMENTATION

A. Shock tube

A shock tube is a relatively simple apparatus which allows for the study of unsteady and high-speed flow phenomena. It is comprised of a high pressure and a low pressure section known as the driver and driven sections, respectively. The two compartments are separated by a thin diaphragm. When the diaphragm is ruptured, either manually or simply by increasing the pressure within the driver section, compression waves are created which propagate into the driven section. These wave coalesce and form a shock wave.[21,22] As the shock wave propagates along the driven section it acts like a piston, compressing the gas in the tube. Simultaneously an expansion front travels in the driver section, matching the pressure behind the shock front to the undisturbed gas within the driver section. The gas in the driven section and driver gas make contact at a position referred to as the contact surface, which moves along the tube behind the shock front. The gas to the right of the contact surface is compressed and heated by the shock wave but since the gas to the left of this line has expanded from the compression chamber it has, therefore has been cooled.

A cylindrical shock tube was used in the present study with the driver section manufactured from aluminium with an internal diameter of 40 mm, wall thickness of 5mm, and length of 150 mm. This thickness was chosen since this was the minimum thickness required to sustain the pressures encountered within the shock tube. The driven section was made from PVC tubing with an internal diameter of 20 mm, wall thickness of 5 mm, and total length of 740 mm. The driven section was chosen to be manufactured from PVC to avoid any complications when attaching the high-voltage plasma connections. The pressure within the driver section was increased to 6 bar whilst the pressure within the driven section was ambient (1 bar). Air was used as both the driver and driven gas. A 19 μm Mylar diaphragm was used to separate the driver and driven sections. The thickness was chosen to be the minimum required that would withstand the pressure difference. The driver pressure was gradually increased until the diaphragm burst.

Based on the ratio between the driver pressure P_4, and driven pressure P_1, using Eq.

(1)[23] the theoretical shock Mach number can be deduced as M_s=1.45.

$$\frac{P_4}{P_1} = \left[1 + \frac{2\gamma_1}{\gamma_1 + 1}\left[M_1^2 - 1\right]\right]\left[\frac{1}{1 - \frac{\gamma_4 - 1}{\gamma_1 + 1}\frac{a_1}{a_4}}\left[M_1 - \frac{1}{M_1}\right]\right]^{\frac{2\gamma_4}{\gamma_4 - 1}} \tag{1}$$

Based on the shock Mach number M_s, the induced flow behind the incident shock U_p, can be arrived at using Eq. (2). This results in a flow behind the shock wave of approximately 217 m/s.

$$U_p = \frac{2a_1}{\gamma_1 + 1}\left[M_1 - \frac{1}{M_1}\right] \tag{2}$$

B. Schlieren flow visualisation

Schlieren photography allows for the visualisation of flow phenomena that are invisible or otherwise difficult to capture.[24–26] Side view images of the flow were captured using a 300 W continuous Xenon arc lamp as the light source. The light is passed through a plano-convex lens, 75 mm in diameter and 75 mm focal length, to create a converged light spot. The focused beam passes through a slit of 1 mm opening before expanding to illuminate a parabolic mirror with a diameter of 203.3 mm and 1016 mm focal length. The collimated light beam from the first mirror passes through the test section and is de-collimated by a second parabolic mirror and focused on a knife edge. By controlling the amount of light cut by the knife edge the sensitivity of the schlieren system was adjusted to capture the flow features. Finally, the Shimadzu Hypervision HPV-1 camera was used to capture the images. The camera was able to acquire images up to 1 Mfps, however, for the present case the maximum frame rate required was 16 kfps. This setup has been successfully applied by Zare-Behtash et al.[27] to study similar flow patterns.

C. Flow duration

Figure 1 known as an x-t (displacement-time) diagram shows the location of the various waves and features present in a shock tube, where point 'o' is the location of the diaphragm. The uniform flow time within the shock tube is determined by the arrival of the reflected rarefaction at the location of the plasma actuator. The head of the rarefaction wave initially meets the end wall of the shock tube driver section and reflects back through the oncoming

expansion fan. The reflected head now moves in the same direction as the expanding gas and accelerates through the fan. The head of the reflected rarefaction wave catches up with the contact surface and overtakes it. After overtaking the contact surface the head of the reflected rarefaction wave accelerates due to the increased speed of sound in the shocked region. Based on the one dimensional analysis presented by Gaydon and Hurle,[23] the duration of this uniform flow, Δt, is approximately 400 μs.

D. Plasma generation and power measurements

DBD plasma actuator configured annularly at the exit of the shock tube. It operates in a surface-mode discharge with an asymmetric arrangement of electrodes (one exposed, one encapsulated) separated by a dielectric barrier as shown in Figure 2. The electrodes are made of 74 μm-thick tinned copper foil tape sticking to the outer and inner surface of the shock tube. The widths of the exposed and hidden electrodes are 5 and 50 mm, respectively. The width of the encapsulated electrode has a considerable effect on the plasma extension.[28–31] It has been depicted by Hale et al.[32–35] that for this particular actuator which runs with the specific driving voltage and frequency, the plasma extends up to the downstream edge of the encapsulated electrode. Because the shock tube was made of 5 mm PVC, it acts as a natural dielectric material.

A Volkraft 3610 power supply capable of outputting 360 W is connected to a transformer cascade that provides the high-voltage signal to the actuators. Voltages up to 40 kV_{p-p} (peak to peak) with driving frequencies of up to 30 kHz are obtainable. The magnitude of the transformer cascade output voltage is controlled by varying the voltage output. The circuit board is monitored via National Instruments (NI), PCI-6713, Data Acquisition device (DAQ) by means of the LabView program where the wave shape, driving frequency, modulation frequency and corresponding duty cycles can be controlled. A LeCroy 1:1000 high-voltage probe, calibrated up to 40 kV peak has been used for input voltage monitoring while the current output is monitored using a current probe which is built into the transformer cascade output. A high bandwidth oscilloscope was necessary to record the plasma discharge due to the high frequency nature of the discharge events. Both the voltage and current probes are connected to a Picoscope 3206, 200 MHz digital oscilloscope and the signals are recorded onto a PC terminal. The input voltage supplied to the exposed electrode

and the frequency are kept constant at 15 kV_{p-p} and 10 kHz, respectively. This driving frequency provides a pure sinusoidal input waveform. The transported charge is measured using a 27 nF capacitor between the encapsulated electrode and the ground connection. The Lissajous plot is obtained using a TDS 1002 (60 MHz, 1.0 GS/s) digital oscilloscope.

III. RESULTS AND DISCUSSION

The analysis is broken down into three phases: Phase I: before the interaction takes place; Phase II: during the passage of the shock wave over the actuator and the initial stage of shock diffraction; Phase III: shock diffraction and depletion of the high velocity air from the shock tube. The different phases are represented graphically in Figure 3.

Figure 4 compares the voltage graphs of the standard DBD at the different phases of the flow for 15 kV_{p-p} and 10 kHz. The input voltage shows consistent repeatability at each phase.

Presence of electronegative gases in air such as oxygen and water vapor efficiently quench nitrogen metastable species and makes a non-uniform microdischarge DBD in atmospheric pressure.[36–38] The properties of these microdischarges have been studied extensively in literature.[39–41] Current pulses always occur at the voltage-rising half-cycle. The 'patchy' appearance of the current trace, such as those presented in Figure 5(a), is due to the presence of these microdischarges, and correspond to the creation of plasma. The more microdischarges are deposited on the surface the more plasma will be present on the actuator. The spikes and the following humps observed in every current half cycle are due to the specific actuator setup employed in the present study, which uses PVC as barrier, rather than a result of the interaction with the flow because they are present in all the phases of the interaction. The current waveform of the microdischarges is characterised by discrete current spikes with usually nano or microsecond duration.[42,43] The presence of uniform plasma characterised by lack of filaments[44] can be observed in Figure 5(b).

The global discharge current varies widely during the passage of the shock wave and the accompanying flow. Instantaneous analysis of the current trace reveals three different plasma structures corresponding to specific characteristics encountered in each run.

With the sinusoidal excitation, the conventional behavior of the current trace is identical to that presented in Figure 5 which also corresponds to the instant before the shock wave-

plasma interactions. Microdischarges occur on both polarities (positive- and negative-going) of the discharge cycle. Microdischarges are so small and numerous on the negative-going portion of the discharge cycle that the current they carry appears as a smooth increase over and above the sinusoidal reactive current. In the positive going portion of the cycle the patchiness that is visible in the current trace is the result of microdischarges with an entirely different structure-much more current is carried by fewer events, with a more defined structure versus the diffuse microdischarges on the opposite half-cycle. Before the presence of the defined microdischarges at -1.5 kV_{p-p} a distinct spike corresponding to the diffused microdischarge is visible.

By means of the Lissajous curve plotted for one cycle, the presence of defined microdischarges along the positive going phase, and the diffuse microdischarges along the negative (at +1.5 kV_{p-p}) and positive going (at -1.5 kV_{p-p}) portions of the Lissajous curve in Figure 6 are visible. The different structure of microdischarges presented in the figure correspond to the current pulses in Figure 5(a).

Immediately after the first phase, no patchiness is present in the current trace for almost 500 μs, as can be seen in Figure 7. This period includes the passage of the shock wave (100 μs) and the duration of uniform high pressure flow behind the shock (400 μs). However, the diffused microdischarges are still present in both half-cycles of the current trace. According to the Mach number of the shock wave, the time it takes for the shock wave to traverse the 50 mm long discharge region is approximately 100 μs and it is indicated by the vertical dashed line in figure.

The boundary layer behind the propagating shock wave is zero at the location of shock front and its thickness increases back through the shock tube.[23] The shock wave propagation produces a discontinuous jump in the neutral density. In a weakly ionized discharge, this neutral density jump creates associated discontinuities in the electron temperature and electron density leading to the formation of a double layer. The generated double layer propagates with the shock front.

As mentioned in section II C the passage of the shock front is followed by a region of relatively uniform flow which lasts about 400 μs. Calculations show that the flow velocity in this region is in the order of 200 m/s. Due to the high free stream velocity the movement of the electrons and ions along the dielectric surface are reduced. This uniform flow also has a high local pressure and density. Therefore, the mean free path (λ) of the particles drops in

this period and the charged particles have less kinetic energy when they collide. This leads to the generation of fewer microdischarges on the surface which leads to reduction of plasma generated by the actuator and quenching of the excited ions.

Following the passage of the shock front and the relatively uniform flow behind over the plasma generated region, the next flow feature that interacts with the plasma are the rarefaction waves that are by this time reflected from the shock tube end wall and are propagating along the shock tube towards the open end. Figure 8, corresponding to Phase III, depicts the current trace of the interaction between these waves and the actuator. As identified in the figure, the interaction between the actuator and rarefaction waves leads to the formation of irregular discharges along the dielectric surface. Similar to the findings of Moreau[2] these irregular discharges are characteristic of streamer propagation where the entire current is concentrated within a few filaments. This behaviour in current trace lasts for 20 ms after which the current pattern returns to its original undisturbed profile similar to that presented in Phase I.

Based on the current and voltage measurements, the power consumption by the actuator is calculated using Equation 3, where T and N represent the time period and the number of cycles, respectively.

$$Power = \frac{1}{NT} \int_{NT} V(t) \cdot I(t) dt \tag{3}$$

Because of the significant reduction of plasma generation due to the interaction with the unsteady flow, a sudden decrease in power consumption from 8.48 W to 8.31 W is observed between the first and second phases. At Phase III this value increases up to 8.57 W. It is conjectured that the increase in power consumption is attributed to maintaining the plasma generated against the back drop of the high speed flow. This behaviour was consistent for the multiple repeats carried out. For validation of the power consumption in the first phase obtained by Equation 3, the Lissajous curve presented in Figure 6 is integrated and multiplied by the applied frequency of the actuator which shows a power consumption of 8.5 W. It was not possible to obtain the Lissajous curves for the Phases II and III. This is because the oscilloscope used did not allow for external triggering for phase locking the flow features with the acquired data.

As the incident shock wave exits the shock tube, the middle portion still remains planar whilst the outer portions which are referred to as the diffracted portion, become curved. A slipstream is created at the shock tube exit due to the separation of the flow which rolls up to

form vortex cores, these features are identified in Figure 9(a). With the passage of time, the precursor shock becomes completely diffracted and because the shock tube is axisymmetric it transforms into a spherical shock wave. The vortex cores grow in size as more fluid is ejected from the shock tube and a vortex ring is visible in Figure 9(b). In Figure 9(c) the diffracted shock has left the field of view and the vortex ring which is a combination of fluid exiting the shock tube and the entrained ambient air has grown in size. A shear layer is created between the flow being ejected from the shock tube and the quiescent ambient air. The shock train visible in the centre of the jet is the mechanism by which the pressure within the jet is balanced to the back pressure. Due to the locally supersonic flow at the centre of the vortex ring, an embedded shock wave is formed which matches the pressure behind the vortex ring to that immediately ahead of it.

The flow velocity within the boundary layer of even supersonic or hypersonic flows is considerably lower than the freestream. Therefore even though the induced flow created by DBD actuators has a relatively low magnitude, when pulsed at certain frequencies it can still have a significant affect on the flow characteristics. Due to the strong electromagnetic interference created by the plasma actuator system it was not possible to obtain quantitative pressure measurements of the flow within the shock nor that of the flow in the immediate exit of the shock tube. However, Figure 10 presents the schlieren results comparing the effect the plasma actuator has on the emerging flow from the shock tube. To help differentiate the effect of the plasma, a schematic of the flow features is also presented in the aforementioned figure. The induced flow by the actuator is due to the movement of the ions created by the voltage supplied to the exposed electrode. The net effect of this movement creates a horizontal jet which inserts momentum and therefore energy to the surrounding environment. As it is visible in the figure, the presence of the vertical suction at the exposed electrode vicinity and the horizontal induced jet opposing the flow created by the actuator leads to the turbulisation of the shear layer created between the emerging and ambient fluid.

Experiments were also carried out by swapping the connection between the exposed and encapsulated electrodes. The only noticeable difference was the switching of the characteristic observed for the positive and the negative going half cycles. For example, the small and numerous microdischarges present on the negative going portion of the discharge cycle were present on the positive going portion of the cycle and the patchiness due to the higher current carried by microdischarges appears on the negative going part of the cycle as

opposed to the positive going. Other than this, the characteristics observed in the current traces were identical to those presented for the original actuator configuration.

IV. CONCLUSIONS

In this special configuration of DBD plasma actuator which used PVC as dielectric material different structures of microdischarges were observed in the positive and negative going portions of the applied voltage. Defined microdischarges were present on the positive going whereas diffused microdischarges were observed on the negative going portion of the cycle. The Lissajous curve also showed these structures clearly.

The influence of the passage of a shock front and the high-speed flow behind it on the characteristics of a DBD actuator were investigated. Good repeatability in voltage signal was observed during the passage of this unsteady flow over the plasma actuator. For ease of analysis, the flow is divided into three distinct phases based on the current trace signal: Phase I: before the interaction, Phase II: during the passage of the shock front and following jet, Phase III: interaction of the shock tube rarefaction waves with the actuator. Throughout these instances the different types of plasma generated was traceable from the presence of microdischarges on current trace.

During the interaction of the shock wave and the induced flow behind it, examination of the current trace showed a significant reduction in microdischarges on the actuator. This implies the reduction of plasma created by the actuator. This behaviour continued until the arrival of the rarefaction waves from the shock tube end wall, namely Phase III. During this phase, irregular discharges appeared on the current signal which would imply the gradual recovery of the actuator. Upon the complete evacuation of the shock tube flow the current trace shows the same pattern as before the interaction took place with the same characteristic microdischarges.

Schlieren measurements of the flow field outside of the shock tube revealed that the induced opposing flow has a turbulisation effect on the shear layer between the emerging and ambient air.

Switching the wire connection of the exposed and encapsulated electrodes only resulted in swapping the characteristics of the positive and negative going parts of the cycle observed in the current traces.

Further studies are currently under way to provide more quantitative data on how the plasma actuator influences the flow field.

Acknowledgments

The authors are indebted to the technical and administrative staff at The University of Manchester for their assistance. The authors would also like to thank Dr. Hugh Frost and Dr. Tohid Erfani for their technical advice and Mr. Manuel Rios for his technical assistance.

[1] T.C. Corke, C.L. Enloe, and S.P. Wilkinson. Dielectric barrier discharge plasma actuators for flow control. *Annual Review of Fluid Mechanics*, 42:505–529, 2010.

[2] E. Moreau. Airflow control by non-thermal plasma actuators. *Journal of Physics D: Applied Physics*, 40:605–636, 2007.

[3] C. Porter, T. McLaughlin, C. Enloe, G. Font, J. Roney, and J. Baughn. Boundary Layer Control Using a DBD Plasma Actuator. In *45th AIAA Aerospace Sciences Meeting and Exhibit, Reno, Paper Number AIAA-2007-786*, 2007.

[4] D.F. Opaits, D.V. Roupassov, S.M. Starikovskaia, A.Y. Starikovskii, I.N. Zavialov, and S.G. Saddoughi. Plasma control of boundary layer using low-temperature non-equilibrium plasma of gas discharge. *AIAA Journal*, 1180(43):10–13, 2005.

[5] I.G. Boxx, R.B. Rivir, J.M. Newcamp, and N.M. Woods. Reattachment of a separated boundary layer on a flat plate in a highly adverse pressure gradient using a plasma actuator. In *3rd AIAA Flow Control Conference, San Francisco, Paper Number AIAA-2006-3023*, 2006.

[6] J. Jacob, R. Rivir, C. Carter, and J. Estevadeordal. Boundary layer flow control using ac discharge plasma actuators. In *AIAA 2nd Flow Control Meeting, AIAA Paper 2128*, 2004.

[7] G.I. Font. Boundary layer control with atmospheric plasma discharges. *AIAA Journal*, 44(7):1572–1578, 2006.

[8] M.L. Post and T.C. Corke. Separation control on high angle of attack airfoil using plasma actuators. *AIAA Journal*, 42(11):2177–2184, 2004.

[9] J. Huang, T.C. Corke, and F.O. Thomas. Plasma actuators for separation control of low-pressure turbine blades. *AIAA Journal*, 44(1):51–57, 2006.

[10] S. Grundmann and C. Tropea. Delay of Boundary-Layer Transition Using Plasma Actuators. In *46th AIAA Aerospace Sciences Meeting and Exhibit, Paper Number AIAA-2008-1369*, 2008.

[11] A.F. Alexandrov, N.V. Ardelyan, S.N. Chuvashev, A.P. Ershov, A.A. Rukhadze, I.B. Timofeev, B.I. Timofeev, and V.M. Shibkov. Supersonic plasma flows and their influence on aerodynamics of flight. *Journal of Technical Physics*, 41:533–550, 2000.

[12] T.C. Corke, D.A. Cavalieri, and E. Matlis. Boundary-layer instability on sharp cone at Mach 3.5 with controlled input. *AIAA Journal*, 40:1015–1018, 2002.

[13] P. Bletzinger, B.N. Ganguly, D. Van Wie, and A. Garscadden. Plasmas in high speed aero-

dynamics. *Journal of Physics D: Applied Physics*, 38:R33, 2005.

[14] J.S. Shang, R.L. Kimmel, J. Menart, and S.T. Surzhikov. Hypersonic flow control using surface plasma actuator. *Journal of Propulsion and Power*, 24(5):923–934, 2008.

[15] P. Bletzinger, B.N. Ganguly, and A. Garscadden. Strong double-layer formation by shock waves in nonequilibrium plasmas. *Physical Review E*, 67(4):047401, 2003.

[16] P. Bletzinger and B.N. Ganguly. Local acoustic shock velocity and shock structure recovery measurements in glow discharges. *Physics Letters A*, 258(4-6):342–348, 1999.

[17] S.O. Macheret, Y.Z. Ionikh, N.V. Chernysheva, A.P. Yalin, L. Martinelli, and R.B. Miles. Shock wave propagation and dispersion in glow discharge plasmas. *Physics of Fluids*, 13:2693, 2001.

[18] B.N. Ganguly, P. Bletzinger, and A. Garscadden. Shock wave damping and dispersion in nonequilibrium low pressure argon plasmas. *Physics Letters A*, 230(3-4):218–222, 1997.

[19] P. Bletzinger, B.N. Ganguly, and A. Garscadden. Influence of dielectric barrier discharges on low mach number shock waves at low to medium pressures. *Journal of Applied Physics*, 97:113303, 2005.

[20] K. Barckmann, S. Grundmann, C. Tropea, and J. Kriegseis. Dielectric-barrier discharge plasmas for flow control at higher mach numbers. 2010.

[21] J.K. Wright. *Shock tubes*. Wiley, 1961.

[22] J.D. Anderson. *Modern compressible flow: with historical perspective*, volume 2. McGraw-Hill Boston, 1990.

[23] A.G. Gaydon and I.R. Hurle. *The shock tube in high-temperature chemical physics*. Reinhold Pub. Corp., 1963.

[24] G.S. Settles. *Schlieren and shadowgraph techniques: visualizing phenomena in transparent media*. Springer Verlag, 2001.

[25] J.S. Oh, O.T. Olabanji, C. Hale, R. Mariani, K. Kontis, and J.W. Bradley. Imaging gas and plasma interactions in the surface-chemical modification of polymers using micro-plasma jets. *Journal of Physics D: Applied Physics*, 44:155206, 2011.

[26] J.W. Bradley, J.S. Oh, O.T. Olabanji, C. Hale, R. Mariani, and K. Kontis. Schlieren photography of the outflow from a plasma jet. *Plasma Science, IEEE Transactions on*, 39(11):2312–2313, 2011.

[27] H. Zare-Behtash, K. Kontis, N. Gongora-Orozco, and K. Takayama. Shock wave-induced

vortex loops emanating from nozzles with singular corners. *Experiments in Fluids*, 49(5):1005–1019, 2010.

[28] M. Forte, J. Jolibois, J. Pons, E. Moreau, G. Touchard, and M. Cazalens. Optimization of a dielectric barrier discharge actuator by stationary and non-stationary measurements of the induced flow velocity: application to airflow control. *Experiments in Fluids*, 43(6):917–928, 2007.

[29] C.L. Enloe, T.E. McLaughlin, R.D. VanDyken, K.D. Kachner, E.J. Jumper, T.C. Corke, M. Post, and O. Haddad. Mechanisms and responses of a single dielectric barrier plasma actuator: geometric effects. *AIAA Journal*, 42(3):595–604, 2004.

[30] R. Erfani, T. Erfani, S.V. Utyuzhnikov, and K. Kontis. Optimisation of multiple encapsulated electrode plasma actuator. *Aerospace Science and Technology*, 2012.

[31] R. Erfani, T. Erfani, C. Hale, K. Kontis, and S.V. Utyuzhnikov. Optimization of Induced Velocity for Plasma Actuator with Multiple Encapsulated Electrodes using Response Surface Methodology. In *49th AIAA Aerospace Sciences Meeting including the New Horizons Forum and Aerospace Exposition, Orlando, Paper Number AIAA-2011-1206*, 2011.

[32] C. Hale, R. Erfani, and K. Kontis. Plasma actuators with multiple encapsulated electrodes to influence the induced velocity. In *48th AIAA Aerospace Sciences Meeting Including the New Horizons Forum and Aerospace Exposition, Paper Number AIAA-2010-1223*, 2010.

[33] C. Hale, R. Erfani, and K. Kontis. Plasma actuators with multiple encapsulated electrodes to influence the induced velocity : Further configurations. In *40th Fluid Dynamics Conference and Exhibit, Paper Number AIAA-2010-5106*, 2010.

[34] R. Erfani, C. Hale, and K. Kontis. The Influence of Electrode Configuration and Dielectric Temperature on Plasma Actuator Performance. In *49th AIAA Aerospace Sciences Meeting including the New Horizons Forum and Aerospace Exposition, Orlando, Paper Number AIAA-2011-955*, 2011.

[35] C. Hale, R. Erfani, and K. Kontis. Increasing the induced velocity of dielectric barrier discharge plasma actuators. CEAS 2009 European Air and Space Conference, 2009.

[36] Z. Fang, J. Lin, X. Xie, Y. Qiu, and E. Kuffel. Experimental study on the transition of the discharge modes in air dielectric barrier discharge. *Journal of Physics D: Applied Physics*, 42:085203, 2009.

[37] A.A. Garamoon and D.M. El-Zeer. Atmospheric pressure glow discharge plasma in air at

frequency 50 hz. *Plasma Sources Science and Technology*, 18:045006, 2009.

[38] C.L. Enloe, T.E. McLaughlin, R.D. VanDyken, K.D . Kachner, E.J. Jumper, and T.C. Corke. Mechanisms and responses of a single dielectric barrier plasma actuator: plasma morphology. *AIAA Journal*, 42(3):589–594, 2004.

[39] V.I. Gibalov and G.J. Pietsch. The development of dielectric barrier discharges in gas gaps and on surfaces. *Journal of Physics D: Applied Physics*, 33:2618, 2000.

[40] B. Eliasson and U. Kogelschatz. Modeling and applications of silent discharge plasmas. *Plasma Science, IEEE Transactions on*, 19(2):309–323, 1991.

[41] K.V. Kozlov, H.E. Wagner, R. Brandenburg, and P. Michel. Spatio-temporally resolved spectroscopic diagnostics of the barrier discharge in air at atmospheric pressure. *Journal of Physics D: Applied Physics*, 34:3164, 2001.

[42] U. Kogelschatz. Dielectric-barrier discharges: Their history, discharge physics, and industrial applications. *Plasma Chemistry and Plasma Processing*, 23(1):1–46, 2003.

[43] Z. Navrátil, R. Brandenburg, D. Trunec, A. Brablec, P. St'ahel, H.E. Wagner, and Z. Kopeckỳ. Comparative study of diffuse barrier discharges in neon and helium. *Plasma Sources Science and Technology*, 15:8, 2006.

[44] F.O. Thomas, T.C. Corke, M. Iqbal, A. Kozlov, and D. Schatzman. Optimization of dielectric barrier discharge plasma actuators for active aerodynamic flow control. *AIAA Journal*, 47(9):2169–2178, 2009.

List of Figures

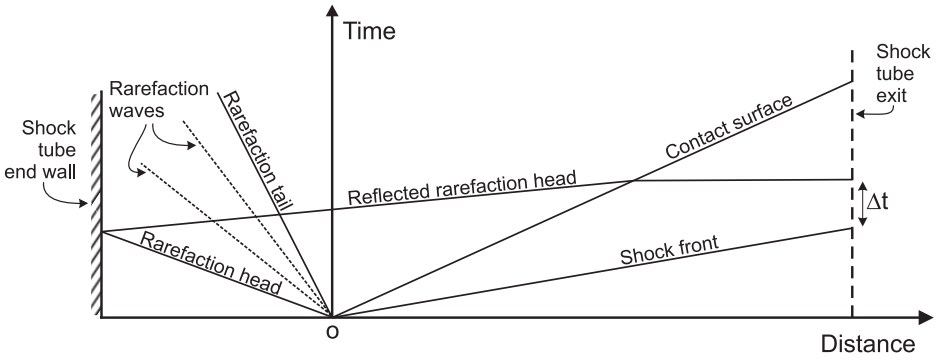

FIG. 1: Shock tube x-t diagram

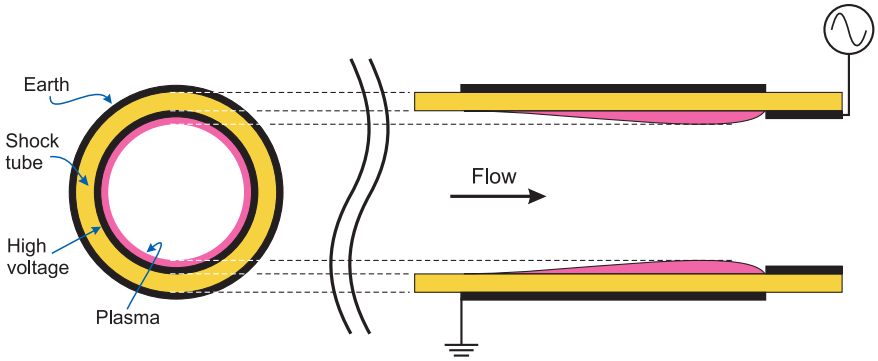

FIG. 2: Standard SDBD actuator configuration placed at the exit of shock tube

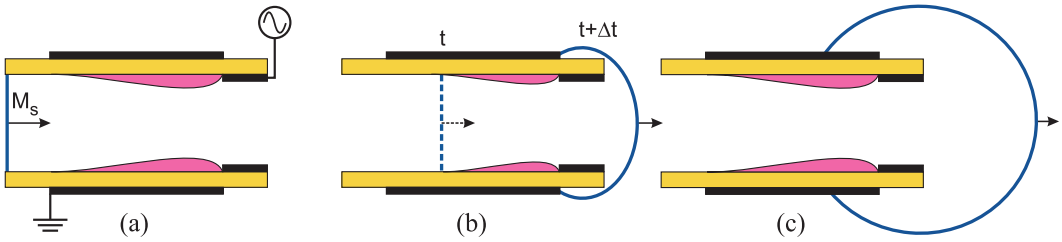

FIG. 3: Three phases of flow according to the position of shock wave respect to the actuator, (a) Phase I, (b) Phase II, (c) Phase III

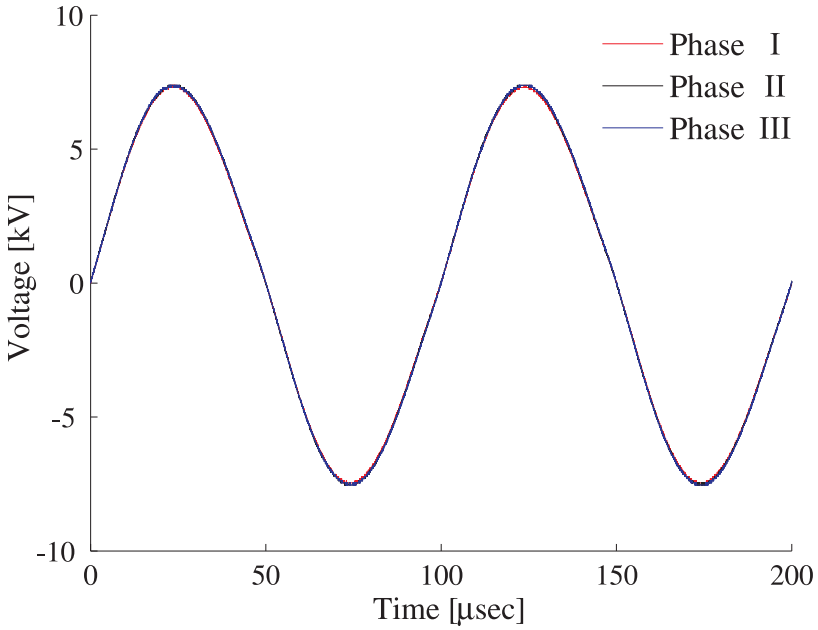

FIG. 4: Traces of the input voltage for three different phases

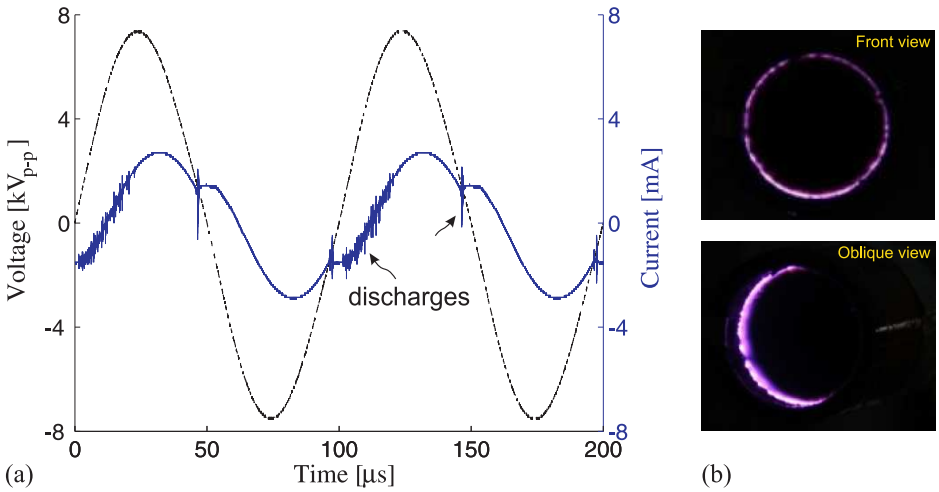

FIG. 5: Current trace for Phase I (a), and plasma generated inside the shock tube (b)

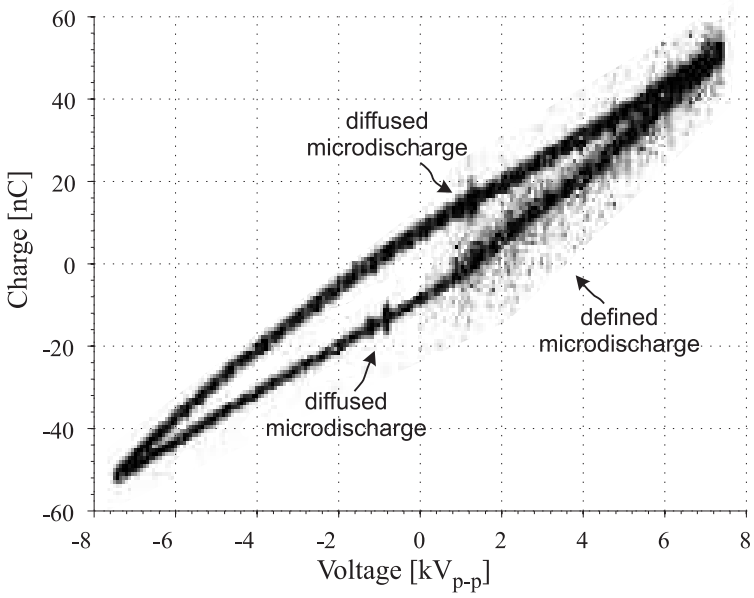

FIG. 6: Lissajous figure corresponding to the first phase

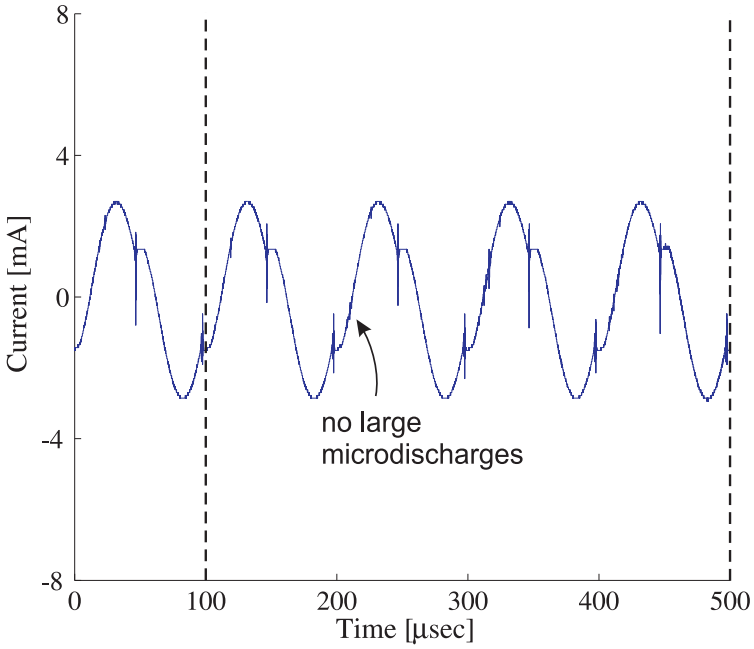

FIG. 7: Current trace for Phase II

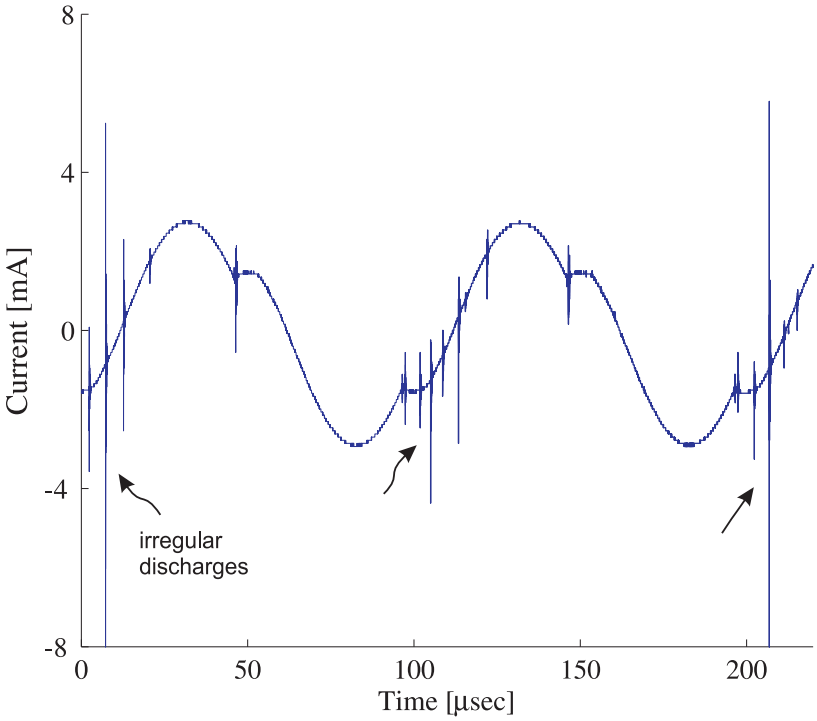

FIG. 8: Current trace for Phase III

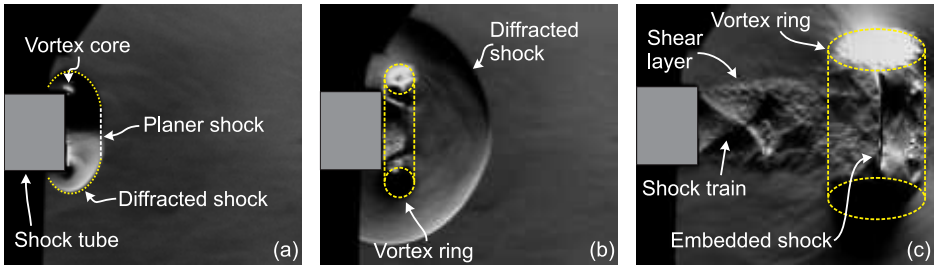

FIG. 9: Time resolved schlieren images of the unsteady flow generated by the shock tube for the plasma off case

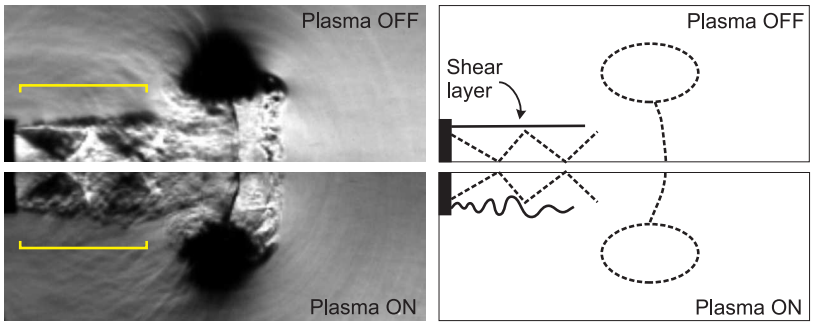

FIG. 10: Schlieren images comparing the plasma off (Top) and plasma on (Bottom) cases